Electronic transport and tip-loading force effect in self-assembled monolayer studied by conducting atomic force microscopy

Hyunwook Song [a], Changjin Lee [b], Yongku Kang [b], Takhee Lee [a],*

[a] *Department of Materials Science and Engineering, Gwangju Institute Science and Technology, Gwangju 500-712, Korea*
[b] *Advanced Materials Division, Korea Research Institute of Chemical Technology, Daejeon 305-600, Korea*

Abstract

Charge transport is investigated for self-assembled monolayers (SAMs) with different molecular structures and various molecular lengths using conducting atomic force microscopy. Conduction mechanism for alkanethiol SAMs is investigated and electronic transport parameters such as barrier height Φ_B and tunneling decay coefficient β are determined and compared with previously reported results. The effects of tip-loading force on metal–SAMs–metal junction properties for different molecular structures are investigated, indicating that molecules with rigid backbone are more resistive to applied loading force than molecules with flexible backbone. Therefore, different aspect of current-voltage characteristics is expected according to molecular structures under the influence of tip loads.
© 2005 Elsevier B.V. All rights reserved.

1. Introduction

Metal–self-assembled monolayers (SAMs)–metal junctions are currently considered as key elements in molecule-based electronic devices pursuing so-called "bottom-up" approach in nanotechnology [1–4]. Thus, characterization of charge transport and conduction mechanism in SAMs has gained particular interest. A full understanding of the electronic transport characteristics through SAMs is essential for any device applications, however such transport measurements are experimentally challenging and intriguing particularly due to the difficulty of making reliable electrical contacts to the nanometer scale monolayers.

Transport studies for these molecular junctions have to date been performed to utilize various methods such as mechanically controllable break junction technique [5], scanning tunneling microscopy (STM) [6], nanopore [7,8], conducting atomic force microscopy (CAFM) [9,10], electromigration nanogap [11,12], cross-wire tunnel junction [13], mercury-drop junction [14],

nanorod [15], and others. Especially, CAFM methods have key advantages for easy accessible junction formation, since no microfabrication process is required. In addition, unlike STM, the CAFM probe provides a direct contact on a sample, so that it eliminates vacuum tunneling effect, ensuring that the voltage is applied fully across the molecular layer between CAFM probe and bottom electrode. Recently, Wold and Frisbie reported CAFM measurements on alkanethiol molecules with various lengths [10]; Cui et al. used Au nanoparticles bound to alkanedithiols in alkanemonothiol matrix in the CAFM measurements [9]. However, in these techniques the CAFM tip might deform the molecular layer, or create additional charge flow paths as well as define a loading force-dependent contact junction area.

In this paper, we have conducted electronic transport measurement of metal–SAMs–metal junctions using the CFAM technique. The careful observations are focused on confirmation of tunneling conduction mechanism for alkanethiol molecules and identification of the effects of tip-induced loading force on junction properties for different molecular structures, especially molecules with rigid backbones versus molecules with flexible backbones.

* Corresponding author. Tel.: +82 62 970 2313; fax: +82 62 970 2304.
E-mail address: tlee@gist.ac.kr (T. Lee).

2. Experiment

2.1. Junction formation of self-assembled monolayers

For our experiments, a ~5 mM solution of alkanethiol and a ~1 mM solution of oligo(phenylene ethynylene) (OPE)-based conjugated molecule with thioacetyl (SAc; SCOCH$_3$) end-group were prepared in ~10 mL ethanol, respectively. The deposition was done on Au surface (Au(250 nm)/Cr(3 nm)/glass) in solution for 1 day inside a nitrogen-filled glovebox with an oxygen level less than 20 ppm. Alkanethiol molecules of various molecular lengths, octanethiol (CH$_3$(CH$_2$)$_7$SH, denoted as C8, for the number of alkyl units), decanethiol (CH$_3$(CH$_2$)$_9$SH, C10), dodecanethiol (CH$_3$(CH$_2$)$_{11}$SH, C12), tetradecanethiol (CH$_3$(CH$_2$)$_{13}$SH, C14) and hexadecanethiol (CH$_3$(CH$_2$)$_{15}$SH, C16), and OPE molecule were used to form the active molecular components. Before use, each sample was rinsed with anhydrous ethanol of a few milliliters and gently blown with dry N$_2$. Metal–SAMs–metal junctions were formed by placing the conductive AFM tips in stationary point contact with the SAM surface under a controlled tip-loading force, as schematically illustrated in Fig. 1. The chemical structure of octanethiol as a representative example of alkanethiols and OPE molecule used in the experiments are shown in Fig. 1.

2.2. CFAM measurement

All measurements were performed using a commercially available AFM system (PSIA, XE-100 model) with conductive AFM tips which were made with Au (20 nm)/Cr(20 nm) coating around conventional AFM tips (nominal force constant of cantilever 0.6 N/m). The mechanical load to CAFM tip was held constant using a standard AFM feedback. Two terminal dc current–voltage ($I(V)$) measurements were performed using a semiconductor parameter analyzer (HP4145B). Voltages were applied to the CAFM tip while the Au substrate was grounded. The tips were not scanned over the surface to avoid mechanical damage to the gold coating around the tips. All electrical measurements in CAFM experiments were carried out at room temperature in ambient environment with humidity control in some degree (20–30% humidity).

Fig. 2. $I(V)$ Characteristics of C12 monolayer junction formed by CAFM tip with loading force of 10 nN. Inset shows the linear regime of $I(V)$ curve within ±0.3 V.

3. Results and discussion

Fig. 2 shows a representative $I(V)$ characteristics obtained from dodecanethiol (C12) SAM formed on Au substrate using the CAFM technique. The applied loading force was 10 nN and $I(V)$ measurement was performed at room temperature and ambient condition over the −1.0 to 1.0 V range. The obtained $I(V)$ curves in this measurement are analogous to the results performed previously [10,16]. A segment of $I(V)$ in a low bias region (particularly inside ±0.3 V) shows linear, thus an ohmic behavior while the overall $I(V)$ shape over the −1.0 to 1.0 V range is sigmoidal, thus overall tunneling behavior (as explained later). $I(V)$ curves for molecular junctions comprised of alkanethiols with different lengths also showed similar curve shapes, even though the absolute current values are strongly dependent on molecular chain length, structure, and tip-loading force [10].

The main conduction mechanism in metal–alkanethiol–metal junction is expected to be a direct tunneling because the Fermi level of contact lies in within the large HOMO-LUMO gap (~8 eV) for short molecular length of alkanethiols [17]. It has been recently shown that tunneling is the main conduction mechanism through alkanethiol SAM in the absence of other parasitic parallel paths from temperature-dependent experiments [8]. To

Fig. 1. Schematics of CAFM characterization method used in this study. Metal–SAMs–metal junction was formed by Au-coated tip. Chemical structures of octanethiol (C8) as an example of alkanehiols and Oligo(phenylene ethynylene) (OPE) based conjugated molecule with thioacetyl (SAc) end-group are displayed. Voltages were applied to the CAFM tip while the Au substrate was grounded.

identify a tunneling behavior of metal–alkanethiol–metal system, one can use the Simmons model, which expresses tunneling current density through a barrier in the tunneling regime of $V < \Phi_B/e$ as [14,18]

$$J = \left(\frac{e}{4\pi^2\hbar d^2}\right)\left\{\left(\Phi_B - \frac{eV}{2}\right)\right.$$

$$\times \exp\left[-\frac{2(2m)^{1/2}}{\hbar}\alpha\left(\Phi_B - \frac{eV}{2}\right)^{1/2}d\right] - \left(\Phi_B + \frac{eV}{2}\right)$$

$$\left. \times \exp\left[-\frac{2(2m)^{1/2}}{\hbar}\alpha\left(\Phi_B + \frac{eV}{2}\right)^{1/2}d\right]\right\} \tag{1}$$

where m is electron mass, d is barrier width determined by molecular length, Φ_B is barrier height, V is applied voltage, and $h = (2\pi\hbar)$ is Planck's constant. For alkanethiol metal–insulator–metal (M–I–M) junctions, the Simmons model has been modified with a parameter α [14]. The α parameter provides either a way of applying the tunneling model of a rectangular barrier to tunneling through a nonrectangular barrier [14] or an adjustment to account for effective mass (m^*) of the tunneling electrons through a rectangular barrier [8,19].

A curve fitting using the Simmons model (Eq. (1)) to describe the tunneling behavior through alkanethiol M–I–M junction is plotted as a solid curve in Fig. 2, demonstrating that the conduction mechanism appears to be tunneling. For this molecular junction, the optimum fitting parameters were found as $\Phi_B = 1.13$ eV and $\alpha = 0.90$.

Particularly in the low-bias region, Eq. (1) can be approximated as [8,18]

$$J \approx \left(\frac{(2m\Phi_B)^{1/2}e^2\alpha}{h^2 d}\right)V \exp\left[-\frac{2(2m)^{1/2}}{\hbar}\alpha(\Phi_B)^{1/2}d\right] \tag{2}$$

where the tunneling decay coefficient β can be defined from $J \approx (1/d)\exp(-\beta d)$ as

$$\beta = \frac{2(2m)^{1/2}}{\hbar}\alpha(\Phi_B)^{1/2} \tag{3}$$

thus, β values can be calculated with Eq. (3) using $\Phi_B = 1.13$ eV and $\alpha = 0.90$ values obtained from $I(V)$ data fittings from which β is determined as $0.98\,\text{Å}^{-1}$

The length-dependent tunneling behavior is examined using alkanethiols with various lengths. Fig. 3 shows a semilog plot of the junction resistance of the low bias regime (-0.3 to 0.3 V) as a function of the molecular length for C8, C10, C12, C14, and C16 alkanethiols at a fixed force of 10 nN. The molecular lengths used in this plot are 13.3, 15.7, 18.2, 20.7, and 23.2 Å for from C8 to C16 alkanethiols. Each molecular length was determined by adding an Au-thiol bonding length to the length of molecule [20]. The error ranges in Fig. 3 were statistically determined from different measurements on various CAFM tip contact positions on SAMs. Inset of Fig. 3 is $I(V)$ curves for alkanethiols with different lengths, which show that current increases with shorter molecular length.

In a low bias tunneling regime, resistance (R) of the junction through alkanethiol SAMs has shown an exponential dependence on the barrier width d as [10]
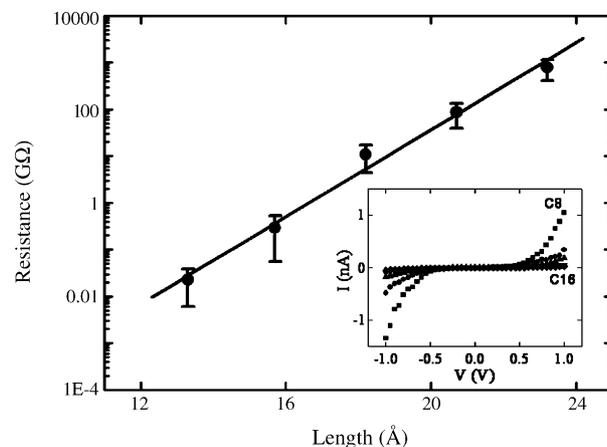
Fig. 3. Semilog plot of junction resistance determined from the low bias regions for C8, C10, C12, C14, and C16 monolayers as a function of molecular length. The line through the data point is exponential fitting, giving a β-value of $1.07 \pm 0.06\,\text{Å}^{-1}$. Inset is $I(V)$ curves for alkanethiols with different lengths.

$$R \propto \exp(\beta d) \tag{4}$$

from this equation, a β value can be determined from the slope of semilog plot in Fig. 3 and can be found as $1.07 \pm 0.06\,\text{Å}^{-1}$. This value is in reasonable agreement with β ($= 0.98\,\text{Å}^{-1}$) calculated from Simmons model fitting of low bias regime (Eq. (3)). This indicates that the Simmons model properly describes tunneling behavior of metal–alkanethiol–metal junction employed in this experiment.

Similarly, from comparison with the results obtained from various test platforms, as summarized in Table 1, one can find that parameters obtained from our CAFM experiments are in reasonable agreement with previously reported values [8,10,16]. This good agreement indicates the validity of the CAFM method in investigating charge transport through monolayers.

However, the current density estimated from our CAFM measurement was found to be smaller than that from previous reported nanopore method [8] by an order of magnitude (see Table 1). We postulate this discrepancy can be because the CAFM tip forms relatively loose physical contact to molecules at low loading force of 10 nN and/or potentially there is water or other contamination layers between CAFM tip and SAM/Au surface in ambient experimental condition.

In addition, there is important consideration to measure $I(V)$ characteristics across monolayers by CAFM, that is, tip-loading force effect which has recently been unfolded to significantly affect junction properties in CAFM test bed [10,16,21]. Generally, the current through the junction increases as the tip-loading force is increased because the contact junction area increases with increasing tip-loading force. If contact junction area increases without any structural deformation of SAMs when tip-loading force is increased, then we can expect that the current density of junctions should remain constant even with increasing loading force. In the following, this assumption will be carefully ascertained by the examination of the current density values dependent on the applied tip-loading force.

Table 1
Summary of alkanethiol tunneling characteristic parameters[a]

Method	β (Å^{-1})	J at 1 V (A/cm^2)	Φ_B (eV)
Nanopore [8]	0.79 ± 0.02[b]	1500 ± 200[d]	1.42 ± 0.04[h]
	0.83 ± 0.04[c]		
CAFM [10]	0.73–0.95	1100–1900[e]	2.2[h]
CAFM [21]	0.64–0.8	10–50[e]	2.3[h]
Tuning fork AFM [31]	1.37 ± 0.03		1.8[i]
Electrochemical [32]	0.97 ± 0.04		
Electrochemical [33]	0.85		
Electrochemical [34]	0.91 ± 0.08		
Theory [35]	0.76	2×10^4 (at 0.1 V)[f]	1.3–3.4[j]
Theory [36]	0.76		
Theory [37]	0.79		
Our experiments by CAFM	0.98[b]	148 at 10 nN[g]	1.13[h]
	1.07 ± 0.06[c]		

[a] Current densities (J) for C12 monothiol at 1 V are extrapolated from published results for other length molecules by using the resistance $R \propto \exp(\beta d)$ relationship.
[b] β-values were calculated from Eq. (3).
[c] β-values were determined from Eq. (4).
[d] Junction areas estimated by SEM.
[e] Junction areas estimated by Hertz model.
[f] Junction area estimated by assuming single molecule.
[g] Junction areas estimated by JKR model (Eq. (5)).
[h] Barrier height Φ_B values were obtained from the Simmons equation.
[i] Barrier height Φ_B values were obtained from bias-dependence of β.
[j] Barrier height Φ_B values were obtained from a theoretical calculation.

The current density may be calculated by estimating a contact junction area for a given loading force. The Johnson–Kendall–Roberts (JKR) contact model is used to evaluate contact area [16,22]. The JKR contact model considers interfacial adhesion force, which can be important at relatively small loads [23]. The Hertz model can be used also in CAFM system [10,21], but neglects the effect due to adhesion force [23]. Therefore, at low loads contact area between two elastic bodies estimated by the Hertz model is considerably smaller than that expected by the JKR model [23]. This reflects the importance of interaction between tip and SAMs under the range of reasonable loading force where there is no collapse of the monolayer structure. According to the JKR contact model, the radius a of contact junction area given by CAFM tip can be expressed by [23,24]

$$a^3 = \left(\frac{R}{K}\right) P_n = \left(\frac{R}{K}\right) \{P + 3\Gamma\pi + (6\Gamma\pi RP + (3\Gamma RP)^2)^{1/2}\} \quad (5)$$

where R is the radius of the CAFM tip which was determined as ~35 nm from scanning electron microscopy study (Fig. 4a) and, where E_1, v_1, E_2, and v_2 are Young's modulus and Poisson's ratio of the sample and Au-coated CAFM tip, respectively. Appropriate E_1, v_1, E_2, and v_2 are not available, but assuming $E_1 \approx 10$ GPa [24,25], $E_2 \approx 69$ GPa [26], and $v_1 \approx v_2 \approx 0.33$ [16,21] compared to similar materials and structure, K may be calculated as ~13 GPa. P_n is the net force, which is sum of applied loading force P and terms due to adhesion force. $\Gamma = 2P_c/3\pi R$ is the adhesion energy per unit area related to adhesion force P_c which can be obtained from force–distance characterization.

(a)

(b)
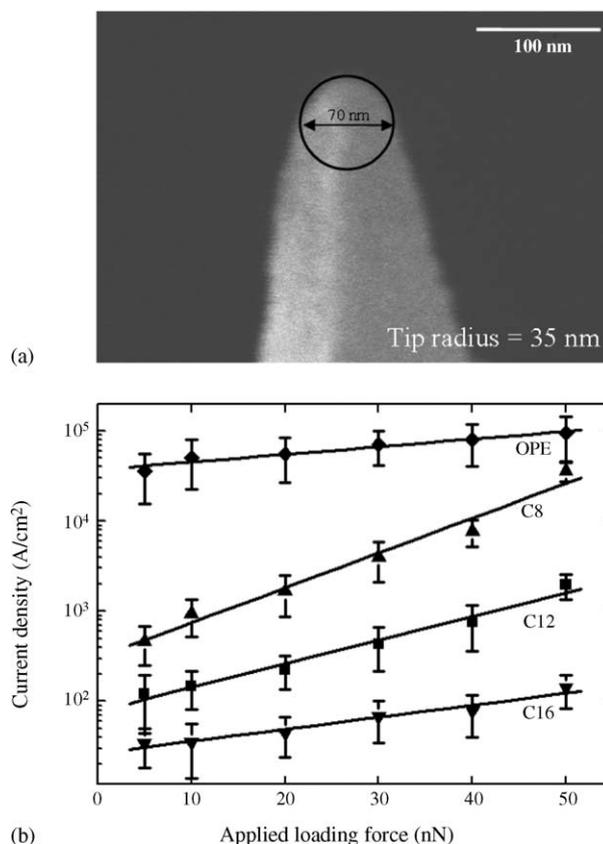
Fig. 4. (a) Scanning electron microscope image of CAFM tip with radius about 35 nm. (b) Semilog plot of current density for C8, C12, C16, and OPE monolayers versus applied loading force at 1.0 V. The sensitivity of the monolayer structure to the tip-induced stress is valuated as the slope of linear fit. Rigid OPE molecule appears to be more resistive to tip loads.

The result clearly shows the increase of the current density with increasing loading force, as shown in Fig. 4b. For example, using Eq. (5), the radii of contact junction areas were estimated as ~5.64, 6.07, 6.43, and 6.74 nm (adhesion force P_c for C12 was determined to be ~12 nN from force–distance characterization) and current densities for C12 at 1.0 V were determined as ~148, 225, 435, and 762 A/cm^2 for applied force of 10, 20, 30, and 40 nN, respectively. The current densities are not constant but increases with increasing loading force.

If a contact tip only increases contact junction area without any structural deformation of SAMs as tip-loading force is increased, then we can expect that the current density of junction should remain constant under increasing loading force. Thus, the observation that current density increased with increasing loading force suggests that increasing current is not simply due to increasing contact junction area and that a potential structural deformation of SAM layer under the tip loads influences the electrical properties of the junctions [10,16,21,27]. For example, one can expect molecular chain is compressed [10] making tunneling distance shorten, or tilted [16,21] resulting in increased chain-to-chain coupling when the tip-loads are applied to molecular layers.

To more specify the effect of molecular structures on $I(V)$ characteristics under tip loads, SAMs having different shape

and length were used. Fig. 4b shows semilog plots of current density for C8, C12, C16, and OPE monolayers as a function of the applied loading force at 1.0 V. The sensitivity of current density to the loading force for different molecular structures can be roughly understood by the slopes in Fig. 4b [22]. Current density is investigated to detect the only element of loading force, but not the increased junction area by tip force. We, again, apply JKR contact theory (Eq. (5)) to evaluate contact area of the junctions. Adhesion force (P_c) of C16, C12, C8, and OPE monolayers employed in the plots of Fig. 4b is determined as 13.5, 12, 10.8, and 21.3 nN from force–distance characterization, respectively. One must note that the slope in Fig. 4b decreases for longer alkanethiols, indicating that the monolayer of longer chain molecules is robust and more resistive to loading forces. The longer alkane chains can stand against tip stress more efficiently because intermolecular interaction between alkanethiol chains (e.g., van der Waals force) is stronger for longer chains, and therefore longer alkanethiols stabilized by van der Waals force attractions can form denser, more compact, and rigid layers than short disordered chains [28]. This tendency agrees with the results of AFM friction measurements [28] and theoretical prediction [29]. In addition, OPE molecules with typical rigid rod-like backbone showed more resistance to the loading force effect than alkanethiols with relatively flexible alkane chain, as the smallest slope was observed for OPE molecules in Fig. 4b. Especially, a comparison of octanethiol and OPE which have almost same molecular length but quite different structure, gives valuable information on the effect of the tip-loading force. The absolute current density of OPE which is conjugated and has delocalized electronic orbitals is higher than that of octanethiol which is nonconjugated and has localized σ-bond orbitals, but the response of current density of OPE molecules to tip loading force is more insensitive and stable. These results reflect that junction current density and the CAFM tip-loading effect depend on the molecular structure.

The junction resistance is also expected to be affected by the contact force [10]. This is because the larger loading force gives more physically compressed SAM. Fig. 5 shows the junction resistance as a function of applied loading force, obtained with the same CAFM tip used for dodecanethiol (C12) SAM, which indicates the junction resistance decreases with increasing loading force. Also, inset of Fig. 5 displays the plots of resistance versus net force including terms of adhesion force which can be determined from force–distance characterization and our experiment shows adhesion force is ~12 nN for dodecanethiol SAMs. The tip-SAM adhesive force exists when tip is in contact on SAM and can be significant especially at low applied tip loading force, thus the magnitude of the adhesion force should not be neglected [16,22,23]. From the plots the power law exponent is determined as ~3.40, that is, $P_n^{(-3.40)}$. The Hertz model [30] predict that the junction contact area should scale as $(load)^{0.67}$, and therefore the junction resistance can be expected to scale as $(load)^{-0.67}$ [10] because the resistance is inversely proportional to the contact area. The deviation from $P_n^{-0.67}$ indicates that the resistance depends not only on contact area, but also on the deformation of molecular structure [10,16,27], as investigated in the example of current density.
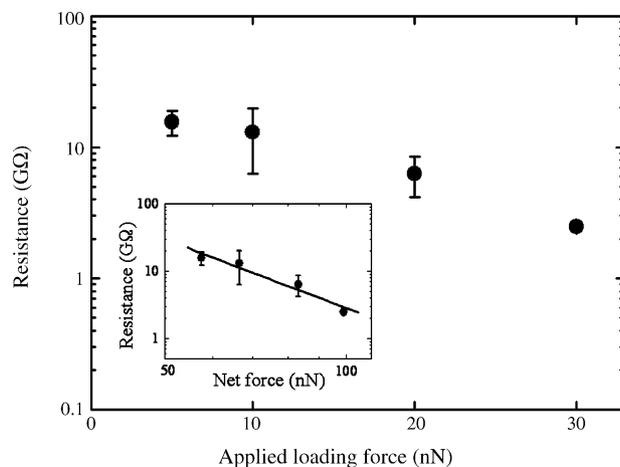
Fig. 5. Semilog plot of the junction resistance of C12 monolayers versus the tip loading force. Inset shows log-log plot of the junction resistance versus net force P_n considering adhesion force. The power law exponent is determined as ~3.40 from the slope of a line fit.

4. Conclusion

Charge transport characterization through metal–SAMs–metal junctions was conducted using CAFM technique. $I(V)$ fitting with Simmons tunneling model and comparison of obtained transport parameters with previous reported values suggest that the main conduction mechanism of alkanethiol molecular junctions formed by CAFM is tunneling. The CAFM tip-loading force was found to dramatically influence the molecular junction properties not only by simply increasing contact junction area but also by a potential structural deformation. Furthermore, $I(V)$ characteristic of junctions was found to be sensitive to molecular structure under tip loads. Junction current of the robust molecules like OPE appears to be more stable and resistive to the tip-induced stress than alkanethiols.

Acknowledgements

References

[1] J.M. Tour, Acc. Chem. Res. 33 (2000) 791.
[2] M.A. Reed, T. Lee (Eds.), Molecular Nanoelectronics, American Scientific Publishers, Stevenson Ranch, 2003.
[3] J.R. Heath, M.A. Ratner, Phys. Today (2003 May) 43.
[4] A. Nitzan, M.A. Ratner, Science 300 (2003) 1384.
[5] M.A. Reed, C. Zhou, C.J. Muller, T.P. Burgin, J.M. Tour, Science 278 (1997) 252.
[6] Z.J. Donhauser, B.A. Mantooth, K.F. Kelly, L.A. Bumm, J.D. Monnell, J.J. Stapleton, D.W. Price Jr., A.M. Rawlett, D.L. Allara, J.M. Tour, P.S. Weiss, Science 297 (2001) 2303.
[7] J. Chen, M.A. Reed, A.M. Rawlett, J.M. Tour, Science 286 (1999) 1550.
[8] W. Wang, T. Lee, M.A. Reed, Phys. Rev. B 68 (2003) 035416.

[9] X.D. Cui, A. Primak, X. Zarate, J. Tomfohr, O.F. Sankey, A.L. Moore, T.A. Moore, D. Gust, G. Harris, S.M. Lindsay, Science 294 (2001) 571.
[10] D.J. Wold, C.D. Frisbie, J. Am. Chem. Soc. 123 (2001) 5549.
[11] J. Park, A.N. Pasupathy, J.I. Goldsmith, C. Chang, Y. Yaish, J.R. Petta, M. Rinkoski, J.P. Sethna, H.D. Abruna, P.L. McEuen, D.C. Ralph, Nature 417 (2002) 722.
[12] W. Liang, M.P. Shores, M. Bockrath, J.R. Long, H. Park, Nature 417 (2002) 725.
[13] J.G. Kushmerick, D.B. Holt, S.K. Pollack, M.A. Ratner, J.C. Yang, T.L. Schull, J. Naciri, M.H. Moore, R. Shashidhar, J. Am. Chem. Soc. 124 (2002) 10654.
[14] R. Holmlin, R. Haag, M.L. Chabinyc, R.F. Ismagilov, A.E. Cohen, A. Terfort, M.A. Rampi, G.M. Whitesides, J. Am. Chem. Soc. 123 (2001) 5075.
[15] J.K.N. Mbindyo, T.E. Mallouk, J.B. Mattzela, I. Kratochvilova, B. Razavi, T.N. Jackson, T.S. Mayer, J. Am. Chem. Soc. 124 (2002) 4020.
[16] T. Lee, W. Wang, J.F. Klemic, J.J. Zhang, J. Su, M.A. Reed, J. Phys. Chem. B 108 (2004) 8742.
[17] M.A. Ratner, B. Davis, M. Kemp, V. Mujica, A. Roitberg, S. Yaliraki, in: A. Aviram, M. Ratner (Eds.), Molecular Electronics: Science and Technology, The Annals of the New York Academy of Sciences, vol. 852, The New York Academy of Sciences, New York, 1998.
[18] J.G. Simmons, J. Appl. Phys. 34 (1963) 1793.
[19] J.K. Tomfohr, O.F. Sankey, Phys. Rev. B 65 (2002) 245105.
[20] D.J. Wold, R. Haag, M.A. Rampi, C.D. Frisbie, J. Phys. Chem. B 106 (2002) 2813.
[21] X.D. Cui, X. Zarate, J. Tomfohr, O.F. Sankey, A. Primak, A.L. Moore, T.A. Moore, D. Gust, G. Harris, S.M. Lindsay, Nanotechnology 13 (2002) 5.
[22] J. Zhao, K. Uosaki, J. Phys. Chem. B 108 (2004) 17129.
[23] K.L. Johnson, K. Kendall, A.D. Robert, Proc. R. Soc. Lond. A 324 (1971) 301–313.
[24] T.P. Weihs, Z. Nawaz, S.P. Jarvis, J.B. Pethica, Appl. Phys. Lett. 59 (1991) 3536–3538.
[25] R. Henda, M. Grunze, A.J. Pertsin, Tribol. Lett. 5 (1998) 191.
[26] M.C. Salvadori, I.G. Brown, A.R. Vaz, L.L. Melo, M. Cattani, Phys. Rev. B 67 (2003) 153404.
[27] K.A. Son, H.I. Kim, J.E. Houston, Phys. Rev. Lett. 86 (2001) 5357.
[28] X. Xiao, J. Hu, D.H. Charych, M. Salmeron, Langmuir 12 (1996) 235.
[29] J. Israelachvili, Intermolecular and Surface Forces, Academic Press, New York, 1992.
[30] K.L. Johnson, Contact Mechanics, Cambridge University Press, 1985.
[31] F.F. Fan, J. Yang, L. Cai, D.W. Price, S.M. Dirk, D.V. Kosynkin, Y. Yao, A.M. Tour, J.M. Rawlett, A.J. Bard, J. Am. Chem. Soc. 124 (2002) 5550.
[32] J.F. Smalley, S.W. Feldberg, C.E.D. Chidsey, M.R. Linford, M.D. Newton, Y.J. Liu, Phys. Chem. 99 (1995) 13141.
[33] K. Weber, L. Hockett, S. Creager, J. Phys. Chem. B 101 (1997) 8286.
[34] K. Slowinski, R.V. Chamberlain, C.J. Miller, M. Majda, J. Am. Chem. Soc. 119 (1997) 11910.
[35] C.-C. Kaun, H. Guo, Nano Lett. 3 (2003) 1521.
[36] S. Piccinin, A. Selloni, S. Scandolo, R. Car, G. Scoles, J. Chem. Phys. 119 (2003) 6729.
[37] J.K. Tomfohr, O.F. Sankey, Phys. Rev. B 65 (2002) 245105.